Near-infrared photon upconversion and solar synthesis using lead-free nanocrystals

Wenfei Liang,[1†] Chengming Nie,[1†] Jun Du,[1†] Yaoyao Han,[1,2] Guohui Zhao,[1,2] Fan Yang,[3] Guijie Liang,[4] and Kaifeng Wu[1,2*]

[1] State Key Laboratory of Molecular Reaction Dynamics, Dalian Institute of Chemical Physics, Chinese Academy of Sciences, Dalian, Liaoning 116023, China.

[2] University of Chinese Academy of Sciences, Beijing 100049, China.

[3] Dalian National Laboratory for Clean Energy, Dalian Institute of Chemical Physics, Chinese Academy of Sciences, Dalian, Liaoning 116023, China

[4] Hubei Key Laboratory of Low Dimensional Optoelectronic Materials and Devices, Hubei University of Art and Science, Xiangyang, Hubei, 441053, China

*Correspondence to: kwu@dicp.ac.cn

Near-infrared to visible photon upconversion holds great promise for a diverse range of applications. Current photosensitizers for triplet-fusion upconversion across this spectral window often contain either precious or toxic elements, and have relatively low efficiencies. Although colloidal nanocrystals have emerged as versatile photosensitizers, the only family of nanocrystals discovered for near-infrared upconversion is the highly-toxic lead chalcogenides. Here we report zinc-doped $CuInSe_2$ nanocrystals as a low-cost and lead-free alternate, allowing for near-infrared to yellow upconversion with an external quantum efficiency reaching 16.7%. When directly merged with photoredox catalysis, this system enables efficient near-infrared-driven organic synthesis and polymerization, which in turn solves the issue of reabsorption loss for nanocrystal-sensitized upconversion. Moreover, the broadband light capturing of these nanocrystals allows for very rapid reactions under indoor sunlight. Extending the reach of "solar synthesis" into the near-infrared may realize the century-long dream of conducting high added-value chemical transformations using sunlight.

Upconversion of near-infrared (NIR) photons to visible photons is of technological relevance to applications across multiple fields.[1-3] In solar energy conversion, upconversion can alleviate the transmission loss of below-bandgap photons and break the Shockley-Queisser efficiency limit of single-junction solar cells.[4] For biomedical imaging, phototherapy or drug delivery, NIR-to-visible upconversion is highly desirable owning to the large penetration depth of the NIR photons into biological tissue.[5] Such a penetration advantage is also appreciated in the context of photoredox organic synthesis and polymerization,[6] as it can overcome the issue of shallow penetration of ultraviolet (UV) and visible photons in the reaction media that limits the reaction rates and the scalability of such systems. Moreover, given the abundance of NIR photons in sunlight, NIR-to-visible upconversion should greatly benefit the field of "solar synthesis" which was envisioned a century ago[7] but has resurged recently for mild, cost-effective and versatile organic transformations.[8]

Sensitized triplet-fusion, or triplet-triplet annihilation photon upconversion (TTA-UC), is a practical pathway to upconvert incoherent, continuous-wave photons such as solar photons.[2-4,9-11] In such systems, photosensitizers capture the incident low-energy photons and then transfer their excited state energy to molecular triplets. Through the fusion of two triplets, a high-energy photon is emitted. Over the years, photochemists have developed a variety of photosensitizers,[12] including but not limited to organic molecules,[13-15] organometallic complexes,[16-18] colloidal nanocrystals (NCs),[19-23] and lead-halide perovskite films[24] or organic bulk-heterojunction films[25]. The materials that can sensitize NIR-to-visible upconversion, however, are not only scarce but also have their own drawbacks. Organometallic complexes with this capability often contain noble metals such as platinum, palladium and osmium.[6,17,18] Pure-organic NIR sensitizers often result in very low upconversion efficiencies.[26] Lead-halide perovskite films are highly-toxic and have limited spectral responses in the NIR (onset at ~750 nm).[24] Colloidal NCs are in principle more diverse in terms of their material composition and spectral tunability, but, to date, the only family of NCs capable of sensitizing NIR-to-visible TTA-UC is lead chalcogenides.[19,27,28]

$CuInSe_2$ NCs and their derivatives have been extensively studied as replacement for lead chalcogenides.[29-31] The avoidance of heavy-metals Cd and Pb , which are under strict regulations, should benefit their widespread use (see Supplementary Text 1). Previously, these NCs have been successfully implemented to solar cells[32,33] and luminescence solar concentrators[34,35]. Here we apply Zn-doped $CuInSe_2$ NCs (abbreviated as ZCISe NCs) as triplet photosensitizers to sensitize NIR-to-visible

TTA-UC. Time-resolved spectroscopy provided direct observation of efficient triplet energy transfer (TET) from trapped-excitons in ZCISe NCs to tetracene ligands on their surfaces. Rubrene molecules were added to accept triplet energy from tetracene ligands and to perform TTA-UC in solution, resulting in NIR-to-yellow upconversion with a record external quantum efficiency of 16.7% (normalized to 100%). Besides, we demonstrated direct engagement of NIR-populated rubrene singlets in photoredox catalysis, a strategy that effectively alleviates the photon reabsorption loss in nanocrystal-sensitized TTA-UC. Further, thanks to the broadband capturing of both NIR and visible photons by the ZCISe NCs, the chemical reactions proceeded rapidly under indoor solar illumination, an especially remarkable example among which is the polymerization of acrylates within just 30 seconds.

Characterization of ZCISe NCs

ZCISe NCs were synthesized using a modified literature method[33]; see Methods for details. These NCs adopt a chalcopyrite phase; see Supplementary Fig. 1. The core-only NCs have an average diameter of 2.8 nm (Supplementary Fig. 2), which were coated with 0.6-nm ZnS shells to form the core/shell NCs with an average diameter of 4.0 nm (Fig. 1a). The thin shells improved the stability of the NCs, yet meanwhile allowing for TET from them. In addition, the ZnS shells can act as encapsulating layers to prevent leakage of the elements from the cores, thus further improving the environmental benignity of the NCs.

The feeding ratio of the Zn dopants in the core synthesis was crucial to the optical properties of NCs. With a feeding molar ratio of Zn:Cu:In = 1:1:1, the NCs dispersed

in hexane display an absorption peak at ~760 nm (determined from the transient-absorption bleach to be presented below), a photoluminescence (PL) peak at ~780 nm and a PL quantum yield (QY) of 21%; see Fig. 1b. The actual elemental ratio of this sample is determined to be Zn:Cu:In:Se ~0.5:0.6:1.1:2 in the core (Supplementary Fig. 3). The nonstoichiometric elemental ratio is typical for this family of materials,[36] which is likely responsible for their rich defect photophysics. Decreasing the Zn feeding ratio can redshift the absorption and PL, but this is accompanied with a decrease in the PLQY (Supplementary Fig. 4). The Zn-induced spectral blueshift indicates that Zn was alloyed with $CuInSe_2$, and the enhanced PLQY highlights the role of Zn in suppressing the formation of nonradiative defect centers, consistent with prior studies.[31-33] If not specified, the sample in Fig. 1b with the highest PLQY was used in the following studies.

We applied time-resolved spectroscopy to study the excited-state dynamics of ZCISe NCs; see Methods for setups. The PL decay of ZCISe NCs in Fig. 1c reveals a long lifetime of hundreds of ns. Such long lifetimes were observed also in closely-related $CuInS_2$-based NCs, and were rationalized as slow radiative recombination between band-edge electrons and self-trapped holes in Cu-related centers.[37-39] For ZCISe NCs herein, however, their transient-absorption (TA) bleach feature, which is known to be dominated by band-edge electrons for this class of materials,[37] shows almost complete decay within 1 ns (Supplementary Fig. 5 and Fig. 1d). In conjunction with the hundreds of ns PL lifetime, this observation suggests that, in addition to previously-known rapid hole self-trapping, the electrons are also localized within 1 ns

into shallow trap states. The slow radiative recombination takes place between trapped electrons and trapped holes.

In a previous study of CISe NC-sensitized solar cells, similar dual trapping pathways of electrons and holes into surface-located electron traps and internal Cu-states, respectively, were also identified.[32] Nevertheless, both the trapped electrons and holes were found to be sufficiently energetic to mediate charge transfer into the TiO_2 electrode and the electrolyte, respectively, thus affording appreciable photon-to-electron conversion efficiencies.[32] Here we examine whether these defects are similarly effective in terms of sensitizing molecular triplets for TTA-UC applications.

Energy transfer from ZCISe NCs

We functionalized the ZCISe surfaces with 5-tetracene carboxylic acid (TCA) as the triplet-acceptor ligands through ligand exchange (see Methods). The triplet energy (E_T) of tetracene is ~1.3 eV (ref[40]), which is lower than the trapped-exciton energy (E_X) of ~1.6 eV in ZCISe (estimated from the PL peak). The absorption spectrum of ZCISe-TCA constructs contains absorption features in the blue range assignable to TCA molecules (Fig. 1b). The original NC absorption is neither reduced nor blue-shifted by TCA, excluding surface corrosion induced by this carboxylate ligand. The number of TCA ligands per ZCISe NC was estimated to be ~25 based on their extinction coefficients and absorbance (see Supplementary Text 2 and Supplementary Fig. 6). Upon TCA functionalization, the PL of ZCISe is quenched by 87% (Fig. 1b). By contrast, functionalization with carboxylated pyrene (E_T ~2.0 eV) or naphthalene

(E_T ~2.6 eV) ligands did not induce any obvious quenching (Supplementary Fig. 7), substantiating that the quenching induced by TCA is not due to introduction of additional surface-trapping states but rather is caused by TET from ZCISe to TCA.

The PL dynamics of ZCISe-TCA displays a quenching efficiency of 91% compared to unfunctionalized ZCISe (Fig. 1c), consistent with steady-state PL. In order to directly observe TET, we studied the TA of ZCISe-TCA. On the ps to ns timescale (Fig. 1d), the bleach of ZCISe decays only slightly faster than unfunctionalized ZCISe, suggesting that the TET process can barely compete with electron-trapping. Interestingly, on the ns to μs timescale (Fig. 1e), after the ZCISe bleach disappears, structured absorption features in the range of 400-500 nm, assignable to $T_1 \rightarrow T_n$ absorption of TCA triplets (^{3}TCA*),[40] gradually emerge. This observation directly evidences TET from "invisible" trapped-excitons of ZCISe to TCA ligands. Fitting the kinetics of the ^{3}TCA* signal yields an average TET time of 14 ns and an average decay lifetime of 134 μs for ^{3}TCA*.

The excited-state processes revealed for the ZCISe-TCA system are summarized in Fig. 1f. Note that the molecular frontier orbitals shown here refer to the first singlet excited-state of TCA (~2.4 eV), whereas the triplet state of ~1.3 eV is phenomenologically shown as lower-energy “intragap” levels, following the convention in previous studies.[41-43] The trapped-exciton energy of ~1.6 eV of the the ZCISe NCs is higher than the triplet energy of TCA but much lower than its singlet energy, which guarantees the selectivity of triplet sensitization.

Sensitized NIR-to-visible upconversion

On the basis of the efficient triplet sensitization of TCA by ZCISe NCs, we further added rubrene molecules to extract triplet energy from TCA ligands and to perform NIR-to-visible TTA-UC, as schemed in Fig. 2a. Experimentally, we excited a deaerated toluene solution containing ZCISe-TCA constructs (~10 μmol/L) and rubrene (16 mmol/L), using an 808-nm continuous-wave laser, and indeed observed yellowish emission from rubrene singlets (Fig. 2b and Fig. 2c); see Methods. The apparent anti-Stokes shift (Δ_{as}), calculated as the energy difference between the first vibronic peak of rubrene emission and the excitation laser, is 0.7 eV (Fig. 2c). The integrated intensity of the yellowish emission increases with excitation power first quadratically and then linearly, with the cross-over point at ~2.1 W/cm^2 defined as the TTA-UC threshold (I_{th}); see Supplementary Fig. 8. Below I_{th}, the concentration of triplets in the system ([^{3}Rub*]) is low and they decay primarily through first-order processes. Thus, [^{3}Rub*] grows linearly with the excitation power and the TTA-UC intensity grows quadratically. Above I_{th}, [^{3}Rub*] becomes sufficiently high such that bimolecular TTA becomes the dominant decay pathway, and thus the TTA-UC intensity grows linearly with the excitation power. Details have been derived and explained in prior studies.[44,45] The TTA-UC quantum efficiency in the linear regime (Φ'_{UC}; normalized to 100%) [46] is calculated to be 16.7 ±0.2% (Fig. 2d). Also included in Fig. 2d are the Φ'_{UC} values of the other two samples (7.0 ±0.1% and 4.8 ±0.2%), exhibiting a general trend of decreasing Φ'_{UC} with decreasing Zn feeding ratio in the core.

We examined the influences of the concentrations of ZCISe-TCA constructs ([ZCISe-TCA]) and rubrene ([Rub]) on the TTA-UC performance. With [Rub] fixed at 16 mmol/L, Φ'_{UC} increases slightly from 16.1% to 16.7% as [ZCISe-TCA] increases from 5 to 10 μmol/L, and then gradually decreases to 7.4% at 40 μmol/L, mainly due to the increasing reabsorption loss of upconversion photons. By contrast, the TTA-UC threshold (I_{th}) monotonically decreases with increasing [ZCISe-TCA], because the sensitized triplet concentration [^{3}Rub*] increases with enhanced absorption of the system at 808 nm. The results are summarized in Table 1; further details are provided in Supplementary Fig. 9 and discussed in Supplementary Text 3. On the other hand, with a fixed [ZCISe-TCA] of 10 μmol/L, the variation of Φ'_{UC} with increasing [Rub] is very minor (Table 1), suggesting that the major reabsorption loss of upconversion photons lies in the ZCISe NCs. The variation of I_{th} is also negligible (Supplementary Fig. 10), as [Rub] does not contribute to absorption at 808 nm. These detailed investigations reveal an intrinsic dilemma between optimizing Φ'_{UC} versus I_{th} for NC-sensitized TTA-UC, due to reabsorption of upconversion photons by broadband absorbing NCs.

The Φ'_{UC} of 16.7 ±0.2% is higher than all prior efficiencies of NIR-to-visible TTA-UC achieved with various types of sensitizers[10], as summarized in Supplementary Table 1 and briefly discussed here. For NC-sensitizers, a pioneering study with PbS NCs reported an efficiency of 1.2%, although it was achieved in solid-state films which are more relevant to device applications and are more challenging than in solution.[19] The initial study with PbSe NCs in solution reported very low efficiency (~0.01%), due to

lack of suitable triplet-transmitters.[20] Later, by using TCA transmitters and optimized NCs, a record efficiency of 11.8% was achieved for PbS QDs.[47] In terms of molecular sensitizers, the Pd- and Pt-complexes in ref[6] generated NIR-to-visible TTA-UC efficiencies of 3.2% and 2.0%, respectively. Other systems using Os-complexes also gave efficiencies of a few per cents.[17,48] A record efficiency of 14.1% for this type of system in ref[18] was achieved by using a Pd-complex sensitizer in conjunction with a newly-developed perylene-based annihilator.

Upconversion for NIR photoredox catalysis

As noted above, the 16.7% efficiency here is an "external" efficiency attenuated by reabsorption of the TTA-UC system itself, especially by ZCISe NCs. The "internal" efficiency for the creation of ^{1}Rub* should be far higher than 16.7%. An alternative strategy to fully exploit the potential of this system is to "in situ" extract the energy of ^{1}Rub* using photoredox reactions (Fig. 3a), thus bypassing the reabsorption loss.[23] An extra benefit of this merged upconversion-photoredox strategy is the excellent penetration of NIR excitation photons through the reaction media and various barriers, as established in ref[6].

The setup for the photoredox reactions is shown in Fig. 3b (left), in which the illumination source is an expanded laser beam with an area of ~0.3 cm^2 at the reactor. As a first test reaction, we conducted reductive dehalogenation of α-bromoacetophenone **1** (Fig. 3c).[49] The concentrations of ZCISe-TCA constructs (~10 μmol/L) and rubrene (16 mmol/L) are identical to the optimized TTA-UC system above, and the concentration of **1** is 0.125 mol/L, corresponding to

photocatalyst molar ratios of 0.08% and 12.8% for ZCISe-TCA and rubrene, respectively. For this reaction, we detected the dehalogenated product **2** in >99% yield within 8 hours illumination by a 400-mW (~1.3 W/cm^2), 808-nm laser (Fig. 3c); see Supplementary Text 4 and Supplementary Fig. 11 for details. All the yields in this work are quantified using gas chromatography-mass spectrometry; see Methods. Control experiments without light or TCA or rubrene resulted in negligible yields, confirming that it is the ^{1}Rub* created from TTA-UC that is driving the reaction. Notably, a previous upconversion-photoredox system requires the addition of a photocatalyst, Eosin Y, to accept the annihilator's singlet energy and to trigger the reaction.[6] By contrast, ^{1}Rub* herein can directly catalyze the reaction without Eosin Y, thus streamlining the reaction system. The second reaction we tested is the oxidation of an amine **3**.[50] Similarly, in ref[6] such a reaction was achieved by adding Rose Bengal as the co-catalyst, but here we achieved 89% yield of product **4** within 8 hours using the upconversion system alone (Fig. 3d and Supplementary Fig. 12). In addition to these simple photoredox reactions, photoreduction of **1** in the presence of phenol **5** triggered a C-O bond formation cross-coupling reaction to produce **6**, with 97% yield within 8 hours (Fig. 3e and Supplementary Fig. 13). The capability of rubrene to simultaneously perform reductive and oxidative photocatalysis arises from its suitable reduction and oxidation potentials (-1.69 and 0.73 V vs SCE, respectively).[51]

We further utilized the upconversion system as the photoinitiator for free-radical polymerization of trimethylolpropane triacrylate (TMPTA) and cationic polymerization of (3,4-Epoxycyclohexane)methyl 3,4-epoxycyclohexylcarboxylate

(EPOX); see Supplementary Text 4 for details. Traditional photoinitiators required UV excitation, and recently there has been increasing interest in developing visible or even NIR-responsive photoinitiators.[52] In our system, because ^{1}Rub* is not energetic enough to directly reduce TMPTA and EPOX monomers, we added diphenyliodonium (Iod) and N-vinylcarbazole (NVK) to activate the reactions.[53] As shown in Fig. 4a, illumination of our upconversion system in the presence of TMPTA and additives with the 808-nm laser resulted in complete formation of polymer gel within 12 minutes. The reaction can be monitored by following the time-dependent IR spectra of the characteristic vibrational bands of the C=C bond in TMPTA (supplementary Fig. 14). Control experiments performed in dark or in the absence of TCA ligands on ZCISe NCs did not form any polymer gel (table in Fig. 4a). Cationic polymerization of EPOX using the merged upconversion-photoredox system was also successful. The complete set of data can be found in Supplementary Figs 15 and 16. The polymerized EPOX can be dispersed with tetrahydrofuran under refluxing at 85 ℃, allowing us to assess its molecular weight (M_n = 11562 g/mol, M_w = 16338 g/mol, dispersity = 1.413).

It is instructive to compare the upconversion system to a system consisting of TMPTA, additives and rubrene excited by a 532-nm laser. The latter showed gel formation in 3 minutes, which is faster because in this case ^{1}Rub* is directly excited by green photons. Accounting for the absorbed photon numbers (using the sample absorptance and laser photon flux), we find the reaction rate of our upconversion system is approximately 6.1% that of the directly-excited rubrene system. This

corresponds to a TTA-UC efficiency of 12.2% by normalizing it to 100% (two NIR photons for one reaction). By contrast, the optical TTA-UC efficiency in Fig. 2d is only ~6.5% at 1.3 W/cm^2; note that the efficiency is power-density dependent and it reaches 16.7% only after saturation. Thus, the TTA-UC efficiency achieved in photoredox reactions is almost 2-fold higher than that revealed by external optical measurements. This enhancement highlights the capability of the merged upconversion-photoredox system to bypass reabsorption loss of upconversion photons.

The considerations above inspired us to examine the photoredox performances of the concentration-varied TTA-UC systems studied in Table 1, by using reductive dehalogenation of **1** as the probe reaction. With [Rub] fixed at 16 mmol/L, unlike the volcano-type dependence of Φ'_{UC} on [ZCISe-TCA], the chemical yield monotonically increases with increasing [ZCISe-TCA], even after accounting for the increase in photon absorptance at 808 nm (Table 1). For example, as [ZCISe-TCA] increases from 10 to 40 μmol/L, the absorptance is enhanced by 2.8-fold, but the chemical yield increases from 19% in 2 hours to 78% in just 1 hour (approximately 8.2-fold faster). The major reason is that I_{th} is reduced from 3.4 to 0.32 W/cm^2, bringing the power density of 1.3 W/cm^2 used in photocatalysis to the efficiency-saturated regime. While the apparent Φ'_{UC} is only 7.4% for [ZCISe-TCA] of 40 μmol/L, due to strong reabsorption loss, the "internal" efficiency relevant to photocatalysis is much higher. Therefore, unlike measuring photon emission from TTA-UC, for which there exists a trade-off between Φ'_{UC} and I_{th}, the performance of the merged

upconversion-photoredox system simply increases with the sensitizer concentration, before detrimental effects (such as aggregation, quenching and precipitation) set in.

Broadband light absorption for solar synthesis

The broadband capturing of both visible and NIR photons by our ZCISe NCs (Fig. 1b) motivated us to move beyond NIR photoredox and to attempt solar synthesis.[8] To test this idea, we placed our reactors on an indoor window shelf on a typical sunny day (Fig. 3b right). The power density was ~32 mW/cm^2. Remarkably, all the photoredox or polymerization reactions proceeded rapidly under this condition ([ZCISe-TCA] = 10 μmol/L, [Rub] = 16 mmol/L). The photoreduction reaction in Fig. 3c took only 1 hour to attach 91% yield, which greatly exceeded the yields of systems directly deploying either Eosin Y (18% in 1 hour) or rubrene (20% in 1 hour) as photocatalysts. Similarly, the upconversion system achieved 95% yield in 2 hours for amine oxidation (Fig. 3d) and 96% yield in 0.5 hour for C-O bond formation (Fig. 3e), both significantly outperforming directly-excited organic photocatalysts.

Photopolymerization allows for naked-eye visualization of the rapid reaction under sunlight. As shown in Fig. 4b, the upconversion system took less than 30 seconds to form polymer gel of TMPTA. By contrast, the system using rubrene photoinitiators took 2.5 minutes to polymerize. A control with unfunctionalized ZCISe NCs alone did not result in polymerization. The other control with the reactor encapsulated in aluminum foil did not polymerize either, excluding heat-induced polymerization. But it is worth mentioning that, due to the extremely rapid reaction, immediate sunlight exposure already started to induce polymerization (Fig. 4b, rightmost).

The ZCISe NCs are highly stable in the reactions. Using the photoreduction reaction for illustration, the NCs showed no changes in their absorption profile or intensity following 8 hours of continuous illumination by the 400-mW, 808-nm laser or 4 hours of continuous illumination by indoor sunlight (Supplementary Fig. 17).

Summary and outlook

The exceptional performance of our upconversion-photoredox system under sunlight can be attributed to the panchromatic absorption of ZCISe NCs with an onset in the NIR. This represents a radical departure from the previous upconversion-photoredox system using Pd- or Pt-complexes as sensitizers with only a narrow absorption band in the NIR but very weak absorption in the visible.[6] In another word, using these complexes, the absorption is shifted to the NIR rather than being extended to the NIR. Such a design could not benefit solar synthesis the way it works here.

Interest in solar synthesis has recently revived in organic chemistry. However, organic chemists' vision has been largely limited to utilizing visible photons in sunlight with visible photocatalysts.[8] In recent years, the NC research community has developed various types of NCs for organic synthesis or polymerization,[54-57] but these NCs contain heavy-metals Cd or Pb and do not absorb NIR photons. Herein the reach of "solar synthesis" is extended to capture both visible and NIR photons abundant in sunlight through the photochemistry of triplet sensitization and upconversion, with the extra advantage of using Cd- and Pb-free NCs. Moreover, as illustrated above, by utilizing the TTA-generated singlets in the form of organic synthesis rather than photon emission, the photon reabsorption loss that is particularly detrimental to

NC-sensitized TTA-UC can be effectively alleviated. On the basis of these considerations, the merger of lead-free NC-sensitized upconversion with photoredox catalysis potentially represents a new paradigm for solar synthesis.

Methods

Chemicals. Oleylamine (OAm, 70%), 1-octadecene (ODE, 90%), zinc acetate dihydrate ($Zn(Ac)_2 \cdot 2H_2O$, 99%), sulphur powder (S 99.999%) and rubrene (99.999%) were purchased from Sigma-Aldrich. Indium acetate ($In(OAc)_3$, 99.999%) and zinc acetate ($Zn(Ac)_2$, 99.999%) were purchased from Alfa Aesar. Diphenylphosphine (DPP, 98%) was purchased from Energy chemical. Copper iodide (CuI, 99.99%), selenium powder (Se, 99.99%), trimethylolpropane triacrylate (TMPTA), 2-bromoacetophenone, diethyl 2,6-dimethylpyridine-3,5-dicarboxylate (Diludine, 98%), N,N-diisopropylethylamine (DIPEA, 99%), methylbenzothiazolium iodide (98%), phenylmagnesium bromide (1.0 M in THF), bromoacetonitrile, Rose Bengal and Eosin Y were purchased from Aladdin. (3,4-epoxycyclohexane)methyl 3,4-epoxycyclohexylcarboxylate (EPOX, 97%), N-Vinyl carbazole, (NVK, 98%), diphenyliodonium hexafluorophosphate (Iod, 98%) and phenol (99.5%) were purchased from innochem. Hexane, toluene, acetone and *N*,*N*-Dimethylformamide (DMF) were purchased from Tianjin Damao Reagent. 5-tetracene carboxylic acid (TCA) was synthesized as described previously[40].

Preparation of stock solutions. The mixture of Se powder (0.79 g, 0.01 mol) , DPP (2 ml) and OAm (2 ml) was vigorously stirred for 24 h at 50 ℃ to prepare the

DPP-Se stock solution. The $Zn(OAm)_2$ stock solution was prepared by mixing $Zn(Ac)_2 \cdot 2H_2O$ (2.2 g, 1 mol), 10 ml ODE and 10 ml OAm in a 100 mL three-neck flask, which was then heated at 120 ℃ for 20 min under vacuum. The OAm-S stock solution was prepared by mixing sulfur powder (64 mg) and 40 ml OAm in a 100 mL three-neck flask and heated to 90 ℃ for 40 min under vacuum.

Synthesis of Zn-doped $CuInSe_2$ core NCs. The Zn-doped $CuInSe_2$ (ZCISe) core NCs were synthesized according to the literature method with some modifications [33]. In a typical synthesis, $Zn(Ac)_2$ (18.3 mg, 0.1 mmol), $In(Ac)_3$ (29 mg, 0.1 mmol), OAm (3 ml) and ODE (3 ml) were loaded in a 100 mL three-neck flask and then degassed at 80 ℃ for 30 min under continuous stirring. At this point, CuI (19 mg, 0.1 mmol) powder was added into the solution. Subsequently, the mixture was heated to 180 ℃ under N_2 atmosphere. Once the temperature was reached, 0.14 ml DPP-Se stock solution was swiftly injected. The reaction was allowed to proceed at 180 ℃ for 15 min, after which it was cooled to 80 ℃ and the solution was mixed with 10 mL toluene. The obtained ZCISe core NCs were purified by being precipitated out of the mixture using acetone and were re-dispersed in 3 ml hexane. NCs of other Zn-doping ratios were obtained by changing the feeding molar ratio of $Zn(Ac)_2$ relative to CuI and $In(Ac)_3$, with other conditions remaining unchanged.

Synthesis of ZCISe/ZnS core/shell NCs. The purified ZCISe core NCs were mixed with 3 ml OAm, 3 ml ODE, 0.4 ml $Zn(OAm)_2$ and 1 ml OAm-S in a 100 mL three-neck flask. The obtained mixture was bubbled with N_2 at room temperature to remove hexane and then heated to 160 ℃ under N_2 atmosphere. After 1 hour, the

reaction mixture was cooled down and 10 mL toluene was injected when the temperature was reduced to 80 ℃. Acetone was used to separate the ZCISe/ZnS core/shell NCs from the solution and the obtained precipitates were dispersed in 3 mL hexane for further use.

Preparation of ZCISe/ZnS-TCA complexes. In a glovebox (O_2, H_2O < 0.2 ppm), 10 μM ZCISe/ZnS NC hexane solution was mixed with TCA powders followed by stirring for 30 min. The mixture was filtered using a Nylon membrane to obtain a clear solution containing ZCISe/ZnS-TCA complexes.

Characterization of NCs. The transmission electron microscopy (TEM) images were taken with a JEOL 2100F field emission electron microscope operating at 200 kV accelerating voltage. The samples were drop-casted onto the ultra-thin carbon film supported by 200-mesh copper grid. The X-ray diffraction (XRD) patterns were carried out using an Empyrean-100 with CuKα radiation. The scanning rate was set as 10 degree/min. For the elemental analysis, a solution of 20 μL of purified NC sample was digested with 69% nitric acid and diluted to 50 ml with water. The Zn, Cu, In and Se contents were determined by a 7300 DV inductively coupled plasma-optical emission spectrometer (ICP-OES). For the Zn-CISe core, the determined elemental ratio was Zn:Cu:In:Se = 0.5:0.6:1.1:2. For the $Zn_{0.4}$-CISe core, the determined elemental ratio was Zn:Cu:In:Se = 0.3:0.7:1.2:2. For the CISe core, the determined elemental ratio was Cu:In:Se = 0.8:1.3:2.

TTA-UC measurements. In a glovebox, the ZCISe-TCA hexane solution was bubbled with N_2 to remove hexane and equal volume of toluene was added into the

system. Note the solvent was changed to toluene to enable a higher solubility of rubrene in the solution. This mixture was further diluted with toluene to reach concentrations of 10 μmol/L for ZCISe-TCA complexes and 16 mmol/L for rubrene (the concentrations of both can be varied to study their influences on TTA-UC and photoredox performances). The ZCISe-TCA//rubrene mixture was sealed in a 1-cm custom-made airtight cuvette for TTA-UC measurements. An 808-nm *cw* laser was chosen to excite the sample. The laser beam was focused onto the sample by a quartz lens with a beam radius of ~0.07 cm measured by the knife-edge method. Along the axis perpendicular to the excitation laser, a lens system was used to collect the fluorescence, which was fiber-coupled to a spectrometer (Maya2000 pro; Ocean Optics). The wavelength-dependent response of the spectrometer was calibrated previously.

The TTA-UC quantum efficiency (Φ'_{UC}, normalized to 100%) was calculated according to the following equation: $\Phi'_{UC} = 2 \times \phi_{ref} \times \frac{photons\ absorbed\ by\ ref}{photons\ absorbed\ by\ sample} \times \frac{PL\ signal(sample)}{PL\ signal\ (ref)}$, where ϕ_{ref} is the PLQY of the reference (rubrene; PLQY = 98% for 532 nm excitation). The number of photons absorbed by the sample or reference per second were calculated from their absorbance, excitation power and excitation photon energy.

Time-resolved spectroscopy. The femtosecond pump-probe TA measurements were performed using a regenerative amplified Ti:sapphire laser system (Coherent; 800 nm, 70 fs, 6 mJ/pulse, and 1 kHz repetition rate) as the laser source and an ultrafast spectrometer. Briefly, the 800 nm output pulse from the regenerative amplifier was

split in multiple parts. One part was directly used to excite the NIR ZCISe NCs. Another part with less than 10% was attenuated with a neutral density filter and focused into a crystal to generate a white light continuum (WLC) used for probe beam. The probe beam was focused with an Al parabolic reflector onto the sample. After the sample, the probe beam was collimated and then focused into a fiber-coupled spectrometer with CMOS sensors and detected at a frequency of 1 kHz. The intensity of the pump pulse used in the experiment was controlled by a variable neutral-density filter wheel. The delay between the pump and probe pulses was controlled by a motorized delay stage. The pump pulses were chopped by a synchronized chopper at 500 Hz. The samples were placed in 1 mm airtight cuvettes in a glovebox and measured under ambient conditions. Nanosecond TA was performed with the EOS spectrometer (Ultrafast Systems LLC). The pump beam was generated in the same way as the femtosecond TA experiment described above. A different white light continuum (380-1700 nm, 0.5 ns pulse width, 20 kHz repetition rate) was used, which was generated by focusing a Nd:YAG laser into a photonic crystal fiber. The delay time between the pump and probe beam was controlled by a digital delay generator (CNT-90, Pendulum Instruments). The time-resolved PL decay was measured using a home-made TCSPC set-up. The excitation source was a supercontinuum laser with proper optical filters. The PL photons were collected by a lens, filtered and then detected by an avalanche photodiode detector (APD).

The PL and TA decay curves can be fitted by multi-exponential functions. The average lifetime was calculated $<\tau_{ave}>$ according to the equation $< \tau_{ave} >= \frac{\Sigma_i A_i \tau_i}{\Sigma_i A_i}$,

where A_i and τ_i are the amplitude and lifetime, respectively, of the *i-th* exponential component. The static PL quenching efficiency $<Q_{PL}>$ can be calculated as: $< Q_{PL} > = 1 - \frac{PL_{NC-TCA}}{PL_{NC}}$, where $PL_{NC\text{-}TCA}$ and PL_{NC} are the intensities of the PL for NC-TCA constructs and free NCs, respectively. The time-resolved PL quenching efficiency $Q_{TR\text{-}PL}$ can be calculated as: $< Q_{TR-PL} >= 1 - \frac{\tau_{ave,NC-TCA}}{\tau_{ave,NC}}$, where $\tau_{ave,NC\text{-}TCA}$ and $\tau_{ave,NC}$ are the average lifetimes for the NC-TCA and NC, respectively.

Photoredox and polymerization experiments. Details for these experiments are provided in Supplementary Text 4. The products of the photoredox reactions were measured using ^{1}H nuclear magnetic resonance (NMR) spectroscopy on a 700 MHz NMR spectrometer (Bruker 700M Avance III HD), and using gas chromatography-mass spectrometry (GC-MS; Agilent Technologies 8890-7250). The latter was used to quantify the chemical yields by measuring the integrated areas of the reactant and product peaks after reaction. The polymerization reactions were monitored using a Fourier-transform IR spectrometer (Nicolet iS50), and the final products were characterized by gel permeation chromatography (GPC; Malvern Panalytical Viscotek).

References

1 Zhou, B., Shi, B., Jin, D. & Liu, X. Controlling upconversion nanocrystals for emerging applications. *Nat. Nanotechnol.* **10**, 924 (2015).

2 Wen, S., Zhou, J., Schuck, P. J., Suh, Y. D., Schmidt, T. W. & Jin, D. Future and challenges for hybrid upconversion nanosystems. *Nat. Photonics* **13**, 828-838 (2019).

3 Zhou, J., Liu, Q., Feng, W., Sun, Y. & Li, F. Upconversion Luminescent Materials: Advances and Applications. *Chem. Rev.* **115**, 395-465 (2015).

4 Schulze, T. F. & Schmidt, T. W. Photochemical upconversion: present status and prospects for its application to solar energy conversion. *Energy & Environ. Sci.* **8**, 103-125 (2015).

5 Chen, G., Qiu, H., Prasad, P. N. & Chen, X. Upconversion Nanoparticles: Design, Nanochemistry, and Applications in Theranostics. *Chem. Rev.* **114**, 5161-5214 (2014).

6 Ravetz, B. D., Pun, A. B., Churchill, E. M., Congreve, D. N., Rovis, T. & Campos, L. M. Photoredox catalysis using infrared light via triplet fusion upconversion. *Nature* **565**, 343-346 (2019).

7 Ciamician, G. The Photochemistry of the Future. *Science* **36**, 385-394 (1912).

8 Schultz, D. M. & Yoon, T. P. Solar Synthesis: Prospects in Visible Light Photocatalysis. *Science* **343**, 1239176 (2014).

9 Singh-Rachford, T. N. & Castellano, F. N. Photon upconversion based on sensitized triplet–triplet annihilation. *Coord. Chem. Rev.* **254**, 2560-2573 (2010).

10 Bharmoria, P., Bildirir, H. & Moth-Poulsen, K. Triplet–triplet annihilation based near infrared to visible molecular photon upconversion. *Chem. Soc. Rev.* **49**, 6529-6554 (2020).

11 Han, S. *et al.* Lanthanide-doped inorganic nanoparticles turn molecular triplet excitons bright. *Nature* **587**, 594-599 (2020).

12 Yanai, N. & Kimizuka, N. New Triplet Sensitization Routes for Photon Upconversion: Thermally Activated Delayed Fluorescence Molecules, Inorganic Nanocrystals, and Singlet-to-Triplet Absorption. *Acc. Chem. Res.* **50**, 2487-2495 (2017).

13 Wu, W., Guo, H., Wu, W., Ji, S. & Zhao, J. Organic Triplet Sensitizer Library Derived from a Single Chromophore (BODIPY) with Long-Lived Triplet Excited State for Triplet–Triplet Annihilation Based Upconversion. *J Org. Chem.* **76**, 7056-7064 (2011).

14 Singh-Rachford, T. N. & Castellano, F. N. Low Power Visible-to-UV Upconversion. *J. Phys. Chem. A* **113**, 5912-5917 (2009).

15 Wu, T. C., Congreve, D. N. & Baldo, M. A. Solid state photon upconversion utilizing thermally activated delayed fluorescence molecules as triplet sensitizer. *Appl. Phys. Lett.* **107**, 031103 (2015).

16 Islangulov, R. R., Kozlov, D. V. & Castellano, F. N. Low power upconversion using MLCT sensitizers. *Chem. Commun.*, 3776-3778 (2005).

17 Amemori, S., Sasaki, Y., Yanai, N. & Kimizuka, N. Near-Infrared-to-Visible Photon Upconversion Sensitized by a Metal Complex with Spin-Forbidden yet Strong S0–T1 Absorption. *J. Am. Chem. Soc.* **138**, 8702-8705 (2016).

18 Huang, L., Wu, W., Li, Y., Huang, K., Zeng, L., Lin, W. & Han, G. Highly Effective Near-Infrared Activating Triplet–Triplet Annihilation Upconversion for Photoredox Catalysis. *J. Am. Chem. Soc.* **142**, 18460-18470 (2020).

19 Wu, M., Congreve, D. N., Wilson, M. W. B., Jean, J., Geva, N., Welborn, M., Van Voorhis, T., Bulović, V., Bawendi, M. G. & Baldo, M. A. Solid-state infrared-to-visible upconversion sensitized by colloidal nanocrystals. *Nat. Photonics* **10**, 31-34 (2016).

20 Huang, Z., Li, X., Mahboub, M., Hanson, K. M., Nichols, V. M., Le, H., Tang, M. L. & Bardeen, C. J. Hybrid Molecule–Nanocrystal Photon Upconversion Across the Visible and Near-Infrared. *Nano Lett.* **15**, 5552-5557 (2015).

21 Mongin, C., Garakyaraghi, S., Razgoniaeva, N., Zamkov, M. & Castellano, F. N. Direct observation of triplet energy transfer from semiconductor nanocrystals. *Science* **351**, 369-372 (2016).

22 Mase, K., Okumura, K., Yanai, N. & Kimizuka, N. Triplet sensitization by perovskite nanocrystals for photon upconversion. *Chem. Commun.* **53**, 8261-8264 (2017).

23 Han, Y., He, S. & Wu, K. Molecular Triplet Sensitization and Photon Upconversion Using Colloidal Semiconductor Nanocrystals. *ACS Energy Lett.* **6**, 3151-3166 (2021).

24 Nienhaus, L., Correa-Baena, J.-P., Wieghold, S., Einzinger, M., Lin, T.-A., Shulenberger, K. E., Klein, N. D., Wu, M., Bulović, V., Buonassisi, T., Baldo, M. A. & Bawendi, M. G. Triplet-Sensitization by Lead Halide Perovskite Thin Films for Near-Infrared-to-Visible Upconversion. *ACS Energy Lett.* **4**, 888-895 (2019).

25 Izawa, S. & Hiramoto, M. Efficient solid-state photon upconversion enabled by triplet formation at an organic semiconductor interface. *Nat. Photonics* **15**, 895-900 (2021).

26 Fückel, B., Roberts, D. A., Cheng, Y. Y., Clady, R. G. C. R., Piper, R. B., Ekins-Daukes, N. J., Crossley, M. J. & Schmidt, T. W. Singlet Oxygen Mediated Photochemical Upconversion of NIR Light. *J. Phys. Chem. Lett.* **2**, 966-971 (2011).

27 Mahboub, M., Huang, Z. & Tang, M. L. Efficient Infrared-to-Visible Upconversion with Subsolar Irradiance. *Nano Lett.* **16**, 7169-7175 (2016).

28 Gholizadeh, E. M., Prasad, S. K. K., Teh, Z. L., Ishwara, T., Norman, S., Petty, A. J., Cole, J. H., Cheong, S., Tilley, R. D., Anthony, J. E., Huang, S. & Schmidt, T. W. Photochemical upconversion of near-infrared light from below the silicon bandgap. *Nat. Photonics* **14**, 585-590 (2020).

29 Talapin, D. V., Lee, J.-S., Kovalenko, M. V. & Shevchenko, E. V. Prospects of Colloidal Nanocrystals for Electronic and Optoelectronic Applications. *Chem. Rev.* **110**, 389-458 (2009).

30 Sandroni, M., Wegner, K. D., Aldakov, D. & Reiss, P. Prospects of Chalcopyrite-Type Nanocrystals for Energy Applications. *ACS Energy Letters* **2**, 1076-1088 (2017).

31 Yarema, O., Bozyigit, D., Rousseau, I., Nowack, L., Yarema, M., Heiss, W. & Wood, V. Highly Luminescent, Size- and Shape-Tunable Copper Indium Selenide Based Colloidal Nanocrystals. *Chem. Mat.* **25**, 3753-3757 (2013).

32 Du, J., Singh, R., Fedin, I., Fuhr, A. S. & Klimov, V. I. Spectroscopic insights into high defect tolerance of Zn:CuInSe2 quantum-dot-sensitized solar cells. *Nat. Energy* **5**, 409-417 (2020).

33 Du, J., Du, Z., Hu, J.-S., Pan, Z., Shen, Q., Sun, J., Long, D., Dong, H., Sun, L., Zhong, X. & Wan, L.-J. Zn–Cu–In–Se Quantum Dot Solar Cells with a Certified Power Conversion Efficiency of 11.6%. *J. Am. Chem. Soc.* **138**, 4201-4209 (2016).

34 Wu, K., Li, H. & Klimov, V. I. Tandem luminescent solar concentrators based on engineered quantum dots. *Nat. Photonics* **12**, 105-110 (2018).

35 Meinardi, F., McDaniel, H., Carulli, F., Colombo, A., Velizhanin, K. A., Makarov, N. S., Simonutti, R., Klimov, V. I. & Brovelli, S. Highly efficient large-area colourless luminescent solar concentrators using heavy-metal-free colloidal quantum dots. *Nat. Nanotechnol.* **10**, 878-885 (2015).

36 Fuhr, A., Yun, H. J., Crooker, S. A. & Klimov, V. I. Spectroscopic and Magneto-Optical Signatures of Cu1+ and Cu2+ Defects in Copper Indium Sulfide Quantum Dots. *ACS Nano* **14**, 2212-2223 (2020).

37 Han, Y., He, S., Luo, X., Li, Y., Chen, Z., Kang, W., Wang, X. & Wu, K. Triplet Sensitization by "Self-Trapped" Excitons of Nontoxic CuInS2 Nanocrystals for Efficient Photon Upconversion. *J. Am. Chem. Soc.* **141**, 13033-13037 (2019).

38 Berends, A. C., Rabouw, F. T., Spoor, F. C. M., Bladt, E., Grozema, F. C., Houtepen, A. J., Siebbeles, L. D. A. & de Mello Donegá, C. Radiative and Nonradiative Recombination in

CuInS2 Nanocrystals and CuInS2-Based Core/Shell Nanocrystals. *J. Phys. Chem. Lett.* **7**, 3503-3509 (2016).

39 Knowles, K. E., Hartstein, K. H., Kilburn, T. B., Marchioro, A., Nelson, H. D., Whitham, P. J. & Gamelin, D. R. Luminescent Colloidal Semiconductor Nanocrystals Containing Copper: Synthesis, Photophysics, and Applications. *Chem. Rev.* **116**, 10820-10851 (2016).

40 Huang, Z., Xu, Z., Mahboub, M., Li, X., Taylor, J. W., Harman, W. H., Lian, T. & Tang, M. L. PbS/CdS Core–Shell Quantum Dots Suppress Charge Transfer and Enhance Triplet Transfer. *Angew. Chem. Int. Ed.* **56**, 16583-16587 (2017).

41 Thompson, N. J., Wilson, M. W. B., Congreve, D. N., Brown, P. R., Scherer, J. M., Bischof, Thomas S., Wu, M., Geva, N., Welborn, M., Voorhis, T. V., Bulović, V., Bawendi, M. G. & Baldo, Marc A. Energy harvesting of non-emissive triplet excitons in tetracene by emissive PbS nanocrystals. *Nat. Mater.* **13**, 1039-1043 (2014).

42 Luo, X., Han, Y., Chen, Z., Li, Y., Liang, G., Liu, X., Ding, T., Nie, C., Wang, M., Castellano, F. N. & Wu, K. Mechanisms of triplet energy transfer across the inorganic nanocrystal/organic molecule interface. *Nat. Commun.* **11**, 28 (2020).

43 Luo, X., Lai, R., Li, Y., Han, Y., Liang, G., Liu, X., Ding, T., Wang, J. & Wu, K. Triplet Energy Transfer from CsPbBr3 Nanocrystals Enabled by Quantum Confinement. *J. Am. Chem. Soc.* **141**, 4186-4190 (2019).

44 Monguzzi, A., Mezyk, J., Scotognella, F., Tubino, R. & Meinardi, F. Upconversion-induced fluorescence in multicomponent systems: Steady-state excitation power threshold. *Phys. Rev. B* **78**, 195112 (2008).

45 Haefele, A., Blumhoff, J., Khnayzer, R. S. & Castellano, F. N. Getting to the (Square) Root of the Problem: How to Make Noncoherent Pumped Upconversion Linear. *J. Phys. Chem. Lett.* **3**, 299-303 (2012).

46 Zhou, Y., Castellano, F. N., Schmidt, T. W. & Hanson, K. On the Quantum Yield of Photon Upconversion via Triplet–Triplet Annihilation. *ACS Energy Lett.* **5**, 2322-2326 (2020).

47 Huang, Z., Xu, Z., Mahboub, M., Liang, Z., Jaimes, P., Xia, P., Graham, K. R., Tang, M. L. & Lian, T. Enhanced Near-Infrared-to-Visible Upconversion by Synthetic Control of PbS Nanocrystal Triplet Photosensitizers. *J. Am. Chem. Soc.* **141**, 9769-9772 (2019).

48 Sasaki, Y., Oshikawa, M., Bharmoria, P., Kouno, H., Hayashi-Takagi, A., Sato, M., Ajioka, I., Yanai, N. & Kimizuka, N. Near-Infrared Optogenetic Genome Engineering Based on Photon-Upconversion Hydrogels. *Angew. Chem. Int. Ed.* **58**, 17827-17833 (2019).

49 Neumann, M., Füldner, S., König, B. & Zeitler, K. Metal-Free, Cooperative Asymmetric Organophotoredox Catalysis with Visible Light. *Angew. Chem. Int. Ed.* **50**, 951-954 (2011).

50 Mashraqui, S. H. & Kellogg, R. M. 3-Methyl-2,3-dihydrobenzothiazoles as reducing agent. Dye enhanced photoreactions. *Tetrahedron Lett.* **26**, 1453-1456 (1985).

51 Anger, F., Breuer, T., Ruff, A., Klues, M., Gerlach, A., Scholz, R., Ludwigs, S., Witte, G. & Schreiber, F. Enhanced Stability of Rubrene against Oxidation by Partial and Complete Fluorination. *J. Phys. Chem. C* **120**, 5515-5522 (2016).

52 Theriot Jordan, C., Lim, C.-H., Yang, H., Ryan Matthew, D., Musgrave Charles, B. & Miyake Garret, M. Organocatalyzed atom transfer radical polymerization driven by visible light. *Science* **352**, 1082-1086 (2016).

53 Xiao, P., Zhang, J., Graff, B., Fouassier, J. P. & Lalevée, J. Rubrene-Based Green-Light-Sensitive Photoinitiating Systems of Polymerization. *Macromol. Chem. Phys.* **218**, 1700314 (2017).

54 Jiang, Y., Wang, C., Rogers, C. R., Kodaimati, M. S. & Weiss, E. A. Regio- and diastereoselective intermolecular [2+2] cycloadditions photocatalysed by quantum dots. *Nat. Chem.* **11**, 1034-1040 (2019).

55 Zhu, X., Lin, Y., Sun, Y., Beard, M. C. & Yan, Y. Lead-Halide Perovskites for Photocatalytic α-Alkylation of Aldehydes. *J. Am. Chem. Soc.* **141**, 733-738 (2019).

56 Huang, Y., Zhu, Y. & Egap, E. Semiconductor Quantum Dots as Photocatalysts for Controlled Light-Mediated Radical Polymerization. *ACS Macro Lett.* **7**, 184-189 (2018).

57 Huang, C., Qiao, J., Ci, R.-N., Wang, X.-Z., Wang, Y., Wang, J.-H., Chen, B., Tung, C.-H. & Wu, L.-Z. Quantum dots enable direct alkylation and arylation of allylic C(sp3)–H bonds with hydrogen evolution by solar energy. *Chem* **7**, 1244-1257 (2021).

Acknowledgments

K.W. acknowledges financial support from the Chinese Academy of Sciences (YSBR-007), the National Natural Science Foundation of China (22173098, 21975253), the Ministry of Science and Technology of China (2018YFA0208703) and Dalian Institute of Chemical Physics (DICP I 202106).

Author contributions

K.W. conceived the ideas and designed the project. W.L. and J.D. synthesized the samples and characterized them. C.N. and W.L. carried out the photoredox reactions. W.L. and G.L. measured the spectroscopy. Y.H. and G.Z. participated in discussions. F.Y. measured the GC-MS and LC-MS. K.W. wrote the manuscript with contributions from all authors. W.L., C.N. and J.D. contributed equally.

Competing interests: Authors declare no competing interests.

Data and code availability: All data and code are available in the main text or the Supplementary Information and can be obtained upon reasonable request from K.W. (kwu@dicp.ac.cn).

Supplementary Information: Supplementary Texts 1-4; Supplementary Figures 1-17**;** Supplementary Table 1**;** SI References

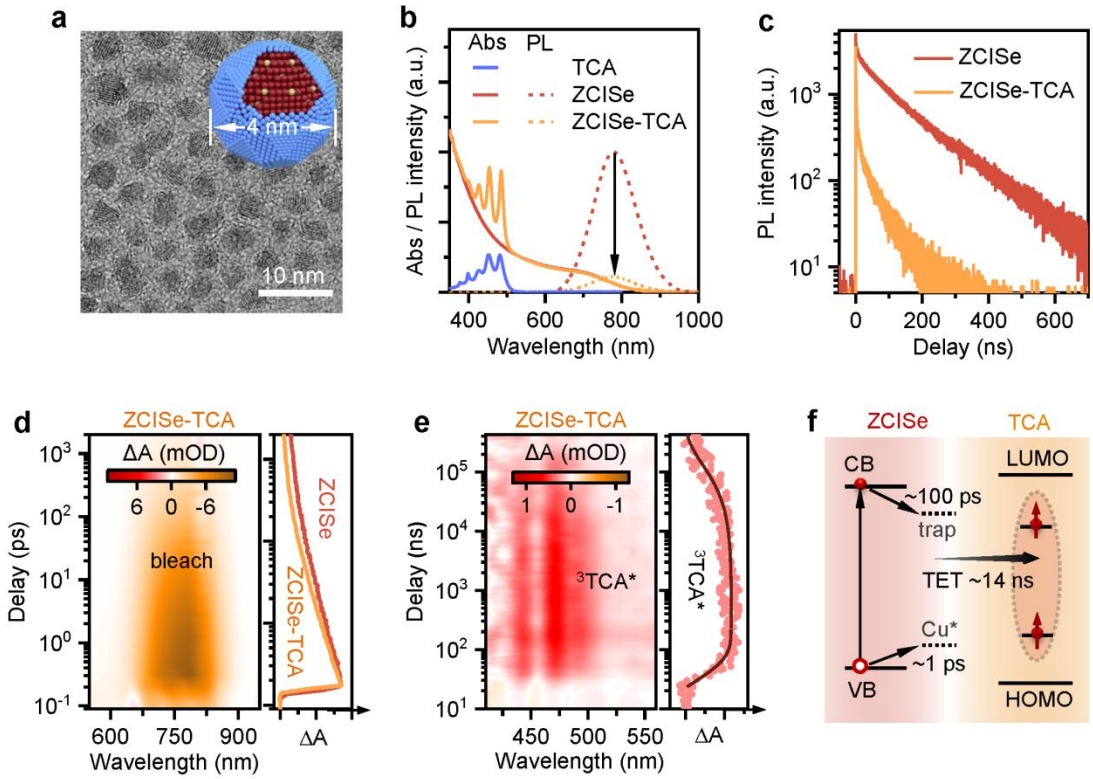

Figure 1. Excited-state dynamics and energy transfer of ZCISe NCs. (a) A representative TEM image of Zn-doped $CuInSe_2$ NCs coated with ZnS shells. Inset is a scheme of the NC structure. (b) Absorption (solid) and PL (dashed) spectra of ZCISe NCs with (orange) or without (red) surface-functionalized TCA ligands, dispersed in hexane. The absorption of free TCA in toluene (blue) is also shown. (c) Time-resolved PL decay of ZCISe NCs with (orange) and without (red) surface-functionalized TCA ligands. (d) 2D pseudo-color TA spectra of ZCISe-TCA within 2 ns following 800 nm excitation. The corresponding kinetics of the bleach center is plotted (orange line), in comparison to that in free ZCISe NCs (red line). (e) TA spectra of ZCISe-TCA from 10 ns to 400 μs following 800 nm excitation. The kinetics of the ^{3}TCA* feature probed at ~485 nm is plotted (red dots) and fitted (black solid line). (f) Scheme of the excited-state dynamics and energy transfer of ZCISe NCs. Note that the frontier orbitals of TCA refer to its first singlet excited-state, whereas the triplet state of ~1.3 eV is phenomenologically shown as lower-energy "intragap" levels.

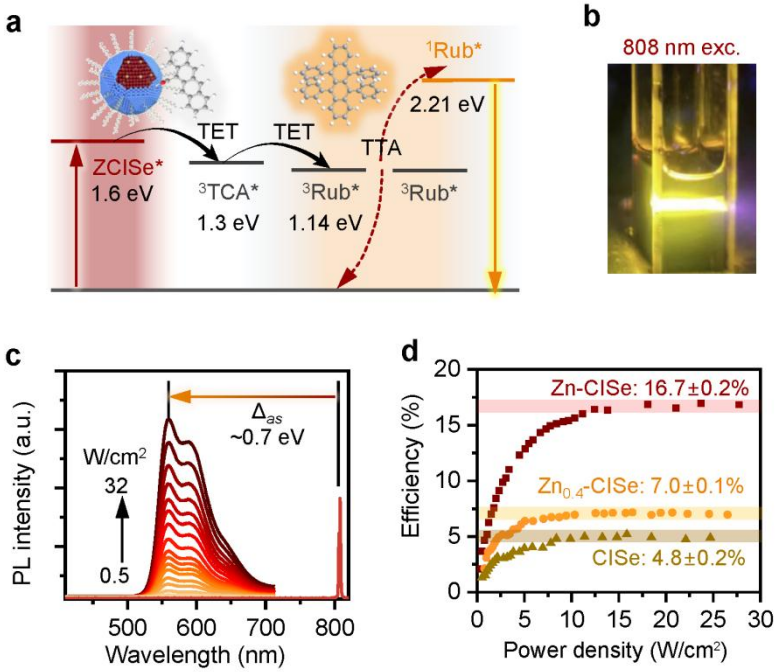

Figure 2. NIR-to-visible TTA-UC. (a) Scheme of the TTA-UC system containing ZCISe sensitizer, TCA transmitter and rubrene annihilator. (b) Photograph of NIR-to-yellow upconversion in an airtight cuvette excited by an 808 nm continuous-wave laser. (c) TTA-UC emission spectra at varying excitation power densities of the 808 nm laser. The apparent anti-Stokes shift is indicated. (d) Normalized TTA-UC quantum efficiencies as a function of power density for the best ZCISe NCs (wine squares) and the other two samples with lower Zn feeding ratios (orange circles and dark yellow triangles). Their average stabilized efficiencies (Φ'_{UC}) are indicated.

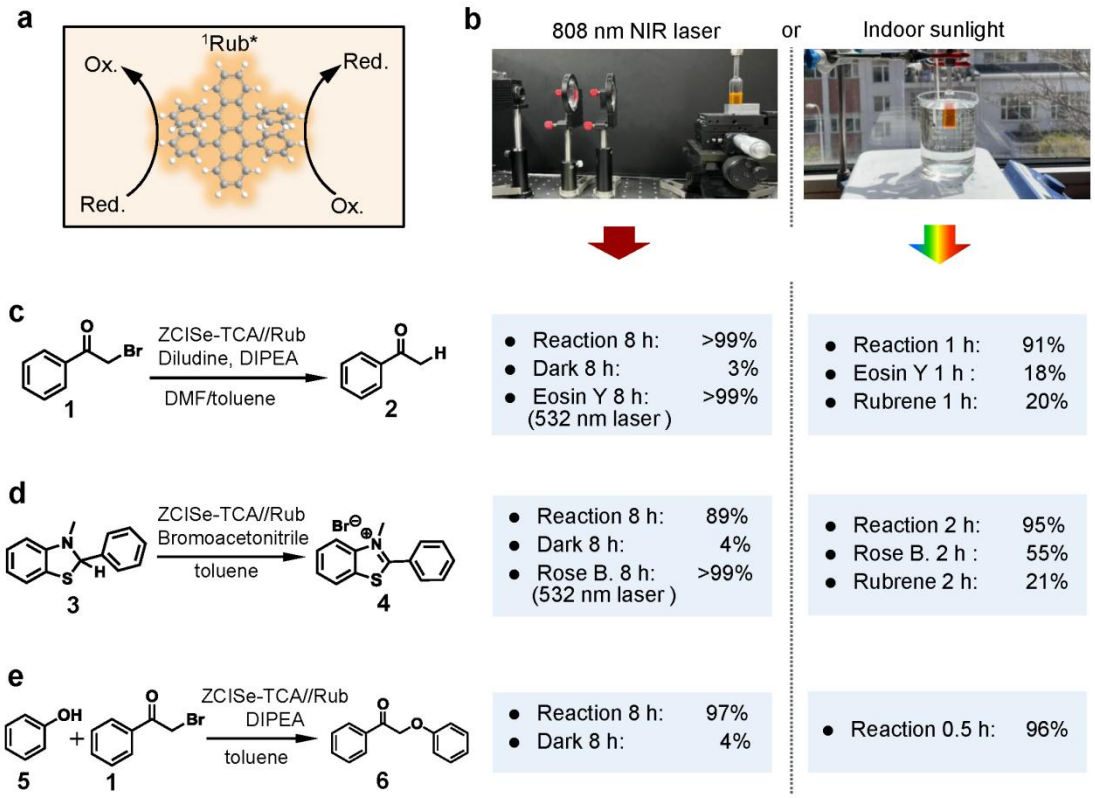

Figure 3. NIR and solar-driven photoredox using TTA-UC. (a) Scheme of merged TTA-UC and photoredox catalysis. (b) Photograph of the reaction setup under, left, 808 nm laser illumination (400 mW; ~1.3 W/cm^2) or, right, indoor solar illumination (~32 mW/cm^2). (c) Reductive dehalogenation of **1** to **2**. The yields and conditions are indicated. Note that a 532 nm (60 mW) laser was used for the direct illumination of Eosin Y photocatalyst to be compared with the 808 nm illuminated TTA-UC system. (d) Oxidation of **3** to **4**. The yields and conditions are indicated. Note that a 532 nm laser was used for the direct illumination of Rose Bengal photocatalyst to be compared with the 808 nm illuminated TTA-UC system. (e) Coupling of **5** with **1** for C-O bond formation. The yields and conditions are indicated.

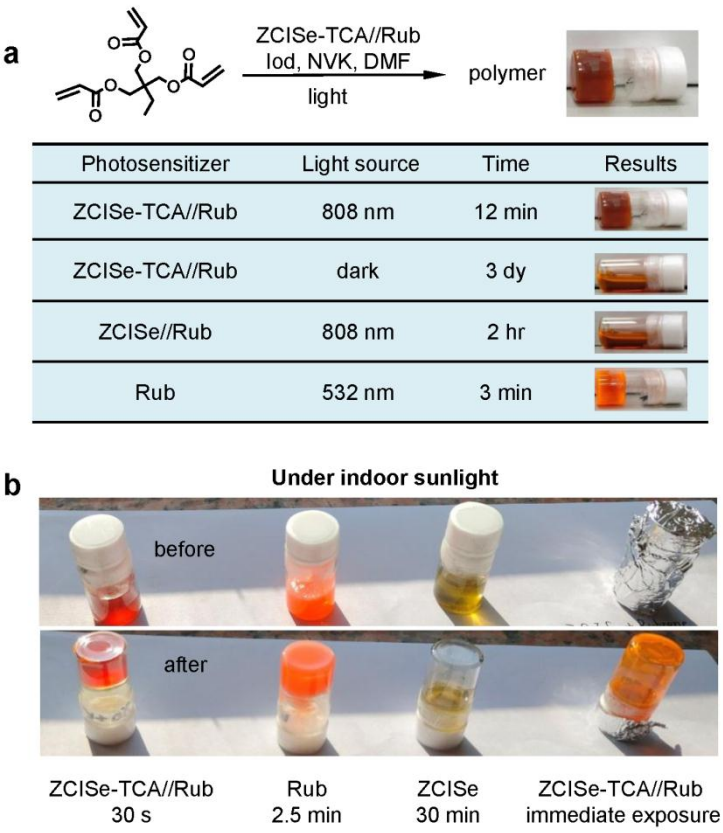

Figure 4. NIR and solar-driven photopolymerization using TTA-UC. (a) Polymerization of TMPTA, and a summary table of experimental conditions and results. (b) Rapid polymerization under indoor sunlight on a window shelf (~32 mW/cm^2). Note that the rightmost sample was covered from sunlight for 30 seconds, but its immediate exposure resulted in polymerization.

Table 1. Influences of sensitizer and annihilator concentrations on TTA-UC and photoredox performances

	Varying [ZCISe-TCA] (μmol/L)[a]				**Varying [Rub] (mmol/L) [b]**		
	5	10	20	40	10	16	40
Φ'_{UC} (%)	16.1	16.7	14.1	7.4	15.2	16.7	16.5
I_{th} (W/cm^2)	3.4	2.1	0.86	0.32	2.2	2.1	2.4
Chemical yield (%)	11 (2 hr)	19 (2 hr)	56 (2 hr)	78 (1 hr)	23 (2 hr)	25 (2 hr)	26 (2 hr)
Absorptance at 808 nm [c]	0.13	0.24	0.42	0.67	0.24	0.24	0.24

[a] [Rub] fixed at 16 mmol/L

[b] [ZCISe-TCA] fixed at 10 μmol/L

[c] Calculated as $1-10^{-OD}$, where OD is the optical density of the ZCISe NCs at 808 nm.